Color center formation in soda-lime glass with femtosecond laser pulses

J. B. Lonzaga, S. M. Avanesyan, S. C. Langford, and J. T. Dickinson[a)]
Physics Department, Washington State University, Pullman, Washington 99164-2814

(Received 3 June 2003; accepted 2 July 2003)

We show that exposure of soda-lime glass to ultrafast laser pulses at 800 nm causes coloration (darkening). We have characterized this coloring with time-resolved measurements of the transmission of 633 nm light through the glass during laser exposure. Reverse processes (partial bleaching) operate on time scales of μs to seconds. The competition between coloration after the femtosecond pulse and the subsequent transmission recovery limits the darkening that can be achieved at a given femtosecond pulse energy and repetition rate. The response of soda-lime glass to 400 and 267 nm ultrafast pulses is quite similar, although much lower pulse energies are required for darkening. We argue that darkening is due to absorption processes that produce mobile charge carriers, which then interact to produce trapped hole centers (H_3^+) that absorb strongly at 633 nm. Trapped electrons (that form *E* centers) are the likely cause of the accompanying loss of transmission in the near ultraviolet. Finally, we show that diffraction gratings can be rapidly and easily produced in this material using holographic methods. © *2003 American Institute of Physics.* [DOI: 10.1063/1.1603962]

I. INTRODUCTION

Laser–material interactions are often enhanced by the presence of defects that absorb at the laser wavelength. Deliberate introduction of defects by mechanical treatments,[1–3] energetic particles[1,4,5] or radiation can be exploited to obtain stronger or more reproducible laser interactions. Undesirable, laser-induced defects can limit the useful lifetime of optical components and influence the use of lasers for analytic chemistry. Laser-induced defects are desirable in many applications, including the exposure of photoresists and the patterning of materials for holographic data storage. In patterning applications, a nonlinear response to the incident light can facilitate the production of well defined features, sometimes with dimensions smaller than the nominal diffraction limit. High intensity, ultrafast lasers have opened up new regimes of laser–material interactions, including defect production and patterning.

In this work we explore the interaction of ultrafast laser pulses with common soda-lime glass. Although this material is not normally considered photosensitive, the high power densities associated with femtosecond pulses can produce nonlinear effects including coloration. Coloration of alkali silicates by exposure to ultrafast laser pulses at 850 nm has been previously reported and attributed to the response of the glass to the short wavelength component of supercontinuum light.[6] In this study we probe this coloration with time-resolved measurements of the transmission of a He:Ne laser beam (633 nm) cofocused with the incident ultrafast laser beam. We show that the initial stages of coloration vary with pulse energy in an extremely nonlinear way—roughly 15th order for 800 nm pulses. Absorption measurements of the ultrafast light indicate that the absorption process itself is only moderately nonlinear—nominally third order. Similar measurements of coloration produced ultrafast pulses at 400 and 267 nm show approximately fifth order variations with fluence, confirming strongly nonlinear behavior even when first order absorption is expected. We attribute these strong nonlinearities to a defect production mechanism that requires high excitation densities; i.e., several excitations are required to produce a single defect. Our results do not support the previously proposed supercontinuum mechanism.[6] Finally, we show that rapid production of diffraction gratings by holographic methods is easily accomplished.

II. EXPERIMENT

The geometry of the transient absorption measurements is indicated schematically in Fig. 1. The output of the femtosecond laser source was focused with a 1 m focal length lens to form a 0.5 mm diam spot on a soda-lime glass slide. The output of a continuous-wave (cw) He–Ne laser was directed obliquely to the femtosecond laser and focused to a 0.1 mm diam spot at the center of the femtosecond laser spot. The intensity of the transmitted He:Ne was detected with a fast photodiode.

Ultrafast laser pulses were provided by a Spectra Physics Hurricane laser system. The laser source was seeded with a Spectra Physics Mai Tai diode-pumped, mode-locked, Ti:sapphire laser. After stretching, the pulse was amplified with a Ti:sapphire regenerative amplifier, pumped with a Spectra-Physics Evolution diode-pumped, *Q*-switched, Nd:$LiYF_4$ laser. Subsequent recompression yielded ~1 mJ pulses at 800 nm with pulse widths less than 130 fs at a repetition rate of 1 kHz. Frequency doubled and tripled radiation was obtained by directing the 800 nm pulses through appropriately phase matched KDP crystals.

Continous wave radiation at 633 nm was provided by a Metrologic model ML-840 7 mW He:Ne laser. After passing through the soda-lime glass slide, the beam transmitted

a)Electronic mail: jtd@wsu.edu

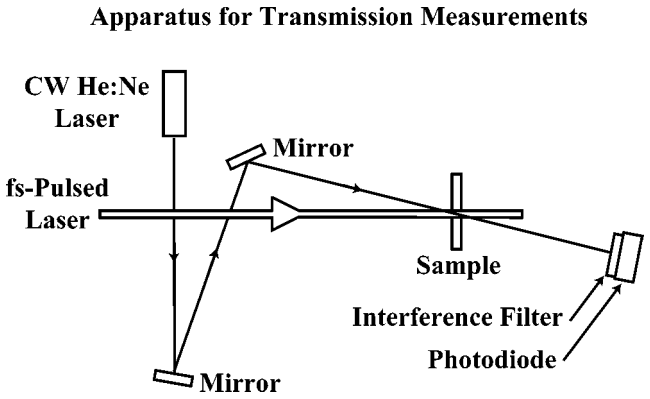

FIG. 1. Apparatus for measuring changes in the transmission of 633 nm light through a soda-lime glass sample during exposure to femtosecond laser pulses. The beam of a continuous-wave He:Ne laser is focused through the femtosecond laser spot.

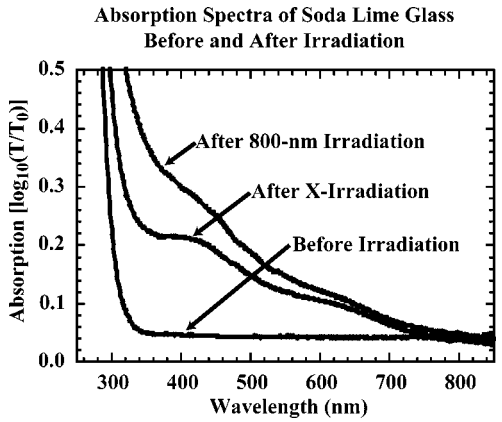

FIG. 2. UV-vis absorption spectra of an untreated soda-lime glass slide, a slide exposed to femtosecond 800 nm radiation, and a slide exposed to Cu $K\alpha$ x rays.

passed through a 633 nm interference filter and was detected with a ThorLabs Det 210 high speed photodiode, with a rise time of 1 ns. The diode output was digitized and recorded with a LeCroy LC584AXL digital oscilloscope with a 1 GHz bandwidth. To maintain maximum sensitivity, an input impedance of 1 MΩ was used in most experiments. The response to fast changes in transmission was limited by a time constant of about 150 μs. Response times of about 10 ns were obtained at an input impedance of 50 Ω, but the reduction in detection sensitivity required very large transmission changes.

Absorption spectra of the colored glass were obtained with a Perkin Elmer Lamba 900 dual beam, ultraviolet/visible (UV/vis) near-infrared (NIR) spectrophotometer. Transmitted light was collected in a 60 mm Spectralon integrating sphere equipped with an extended range photomultiplier tube and a thermostated PbS detector. The use of an integrating sphere insures that forward-scattered light transmitted through the sample is properly detected and included in the measured transmission.

III. RESULTS

A. Absorption spectra of irradiated glass

The absorption spectra of soda-lime glass darkened with femtosecond laser radiation are similar to the absorption spectra of glass darkened with x and γ radiation. Figure 2 displays the absorbance $[\log_{10}(I/I_0)]$ of a 1 mm thick soda-lime glass slide in the 250–800 nm region prior to irradiation, along with soda-lime glass slides darkened with femtosecond laser pulses and Cu $K\alpha$ x-ray radiation from an x-ray diffraction unit. The observed coloration is stable for both types of irradiated samples on the time scale of months. Both darkened samples show broad absorption peaks centered at about 460 and 620 nm. Absorption peaks at these positions are also observed in pure soda silicate glasses[7,8] and soda aluminosilicate glasses[9] exposed to x and γ radiation. In each case, these absorption peaks have been associated with trapped hole centers.[7,8,10] These defects are described in more detail below.

Both femtosecond-and x-irradiated glasses also showed enhanced absorption in the near UV, which is attributed to trapped electron centers.[7,8] Both UV and visible darkening of soda-lime glass showed no measurable loss of absorption on time scales of many minutes to hours after irradiation.

B. Absorption measurements during irradiation

The absorption peak at 620 nm is conveniently near the 633 nm wavelength of a cw He:Ne laser. Transient absorption at 633 nm produced by the ultrafast laser pulses was probed by focusing the beam of the He:Ne laser through the center of the femtosecond laser spot and monitoring the 633 nm beam transmitted with a fast photodiode.

First we show the darkening on a very slow time scale. The transmission signal from a previously unexposed soda-lime glass slide during a 4 s exposure to 620 μJ, 800 nm pulses (1 kHz repetition rate) appears in Fig. 3(a). Irradiation started at time $t=0$ and continued for the duration of data collection. The transmission signal drops rapidly during the first 100 ms (~100 laser pulses) of exposure and then slows gradually.

The transmission signal during the onset of 800 nm irradiation in Fig. 3(a) is shown on a faster time scale in Fig. 3(b). We see the sequence of transmission decreases with successive laser pulses. The digitized drop in transmission signal immediately following the laser pulse is actually faster than the decrease shown here due to a long response time of the detection circuit employed in this experiment ($\leqslant$ 150 μs). Nanosecond time scale measurements of the initial transmission drop are described below. At low pulse energies, the transmission signal after the first laser pulse reaches a plateau and remains constant until the next laser pulse. At higher pulse energies, the transmission signal after the first laser pulse begins to rise prior to the second laser pulse. After exposure to a large numbers of laser pulses, the transmission between laser pulses drops and rises in cyclic fashion, with no net change in transmission.

Transmission during exposure to repeated pulses is history dependent. Under the conditions of this work, the transmission drop following a laser pulse appears to be permanent as long as the cumulative change in transmission signal is

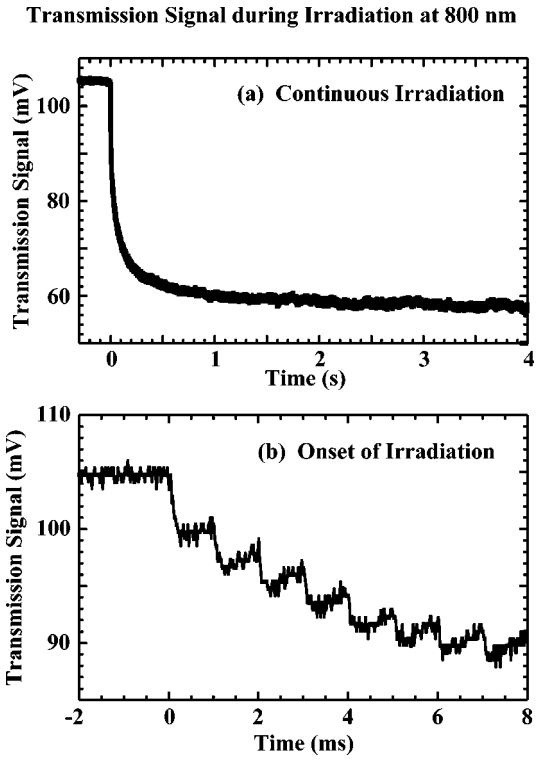

FIG. 3. (a) Smoothed transmission data during exposure to 4000 femtosecond pulses of 800 nm radiation at 620 μJ/pulse, and (b) raw transmission data on a faster time scale during the same experiment showing the onset of irradiation.

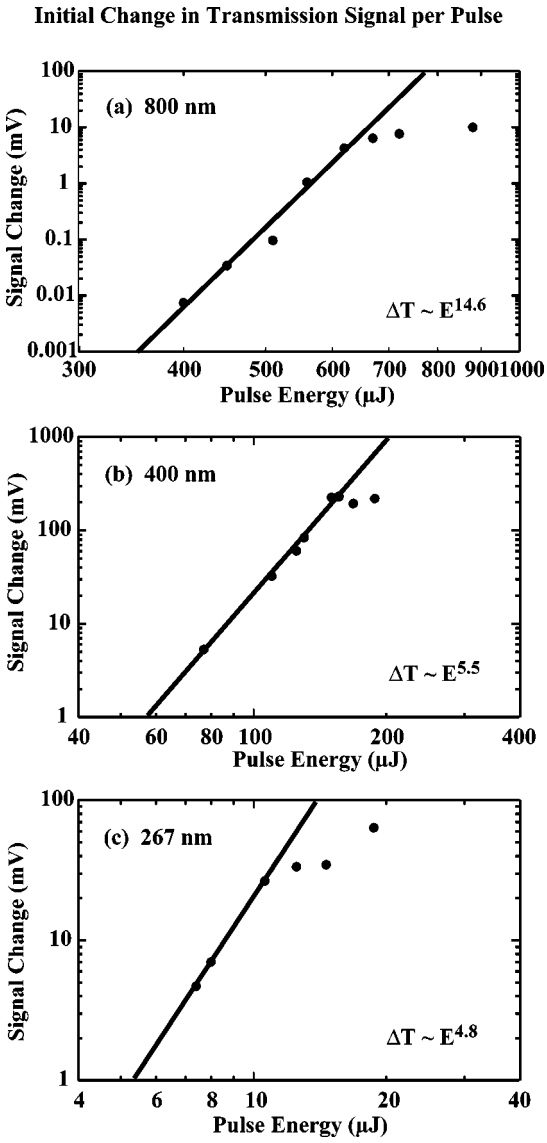

FIG. 4. Initial change per pulse in transmission signal as a function of the pulse energy due to (a) 800, (b) 400, and (c) 267 nm pulses.

less than a few mV. When the cumulative transmission drop exceeds a few mV, the transmission signal develops a distinct minimum and begins to rise until the next laser pulse. We attribute the behavior to the competition between defect creation immediataly after the laser pulse and subsequent defect annihilation. Over the range of pulse energies employed here, this competition limits the maximum transmission change that can be produced by a single laser pulse. After prolonged exposure to femtosecond laser pulses [after 2 or 3 s in Fig. 3(a)], the average transmission changes very slowly.

The time behavior of the transmission changes at 400 and 267 nm is similar to that at 800 nm. At 800 and 400 nm, the observed darkening is relatively uniform throughout the thickness of the glass slide (1 mm thick). At 267 nm, darkening is limited to a surface layer about 300 μm thick, consistent with the poor linear transmission of soda-lime glass at wavelengths below 300 nm.

C. Change in transmission as a function of pulse energy

The magnitude of the peak transmission change at 633 nm is a strong function of pulse energy. To minimize the contribution of defect annihilation processes (recovery in the transmission signal prior to the subsequent laser pulse), we focus on the change in transmission accompanying the first laser pulse, where annihilation is minimized. A plot of the change in the 633 nm transmission signal per ultrafast laser pulse at the onset of irradiation (first pulse only) is plotted as a function of fluence for femtosecond irradiation at 800, 400, and 267 nm in Fig. 4.

At 800 nm, the initial transmission change is an especially strong function of the pulse energy, varying roughly as the pulse energy to the 15th power. At 400 nm, the initial transmission change is a much weaker function of the pulse energy, and varies as the fifth to sixth power of pulse energy. The functional dependence of the transmission change at 267 nm is similar to that at 400 nm. As noted below, this strong function dependence does not necessarily imply a similarly high-order photon absorption process.

At all three wavelengths, the transmission change accompanying the first laser pulse saturates at high pulse energies. At 800 nm, the transmission change saturates at about 10 mV. At 400 nm, the saturation level is much higher, about 200 mV. At 267 nm, the maximum transmission change saturates at an intermediate level. As noted above, the maximum

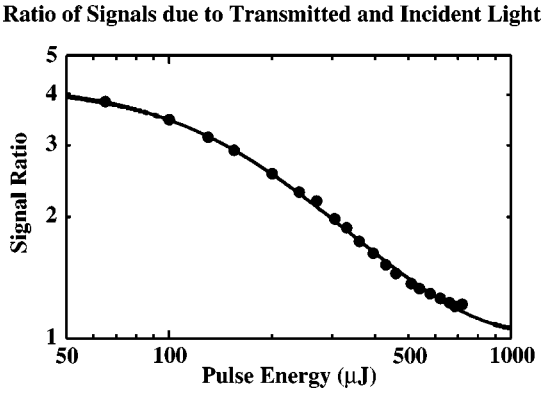

FIG. 5. Log–log plot of the ratio of the signal from a photodiode sampling the transmitted beam to the signal from a photodiode sampling the incident beam at 800 nm. No correction for detector efficiency was made. The gray curve shows the least squares fit of Eq. (1) to the data, which corresponds closely to three-photon absorption.

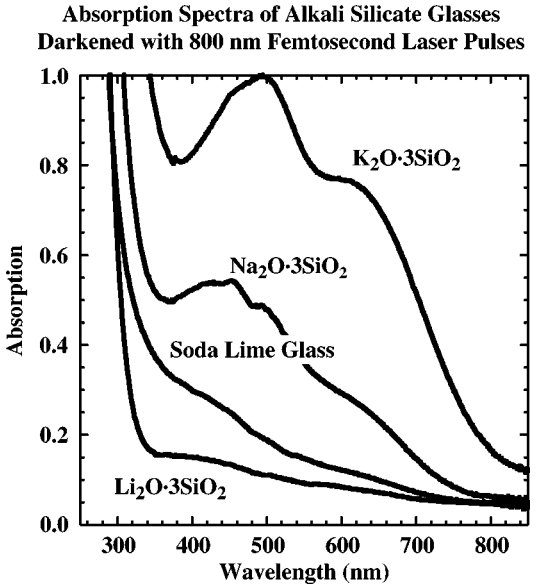

FIG. 6. Absorption spectra of soda-lime glass and three alkali silicate glasses darkened by exposure to femtosecond pulses at 800 nm.

transmission change at 267 nm is limited by the poor transmission of laser light through the sample.

At all three wavelengths, darkening occurs at pulse energies far below the threshold for the production of broadband (supercontinuum) emissions. No discontinuities are observed in the amount of darkening/pulse versus pulse energy (Fig. 4) at the onset of broadband emission. We believe these observations contradict proposed models that require supercontinuum emissions.[6]

D. Absorption at 800 nm

A log–log plot of the transmission of the 800 nm femtosecond laser beam as a function of pulse energy appears in Fig. 5. Assuming power law absorption, the signal I detected through a slab of material as a function of incident intensity energy, I_0 is given by

$$\frac{I}{I_0} = \frac{A}{(1+\alpha \times I_0^{n-1})^{(1/n-1)}}, \tag{1}$$

where the parameter A depends on the detector sensitivity, the parameter α is related to the absorption cross section, and the parameter n is the order of the absorption process. The experimental data requires an additional term proportional to $1/I_0$ to account for small detector offset. A nonlinear least squares curve fit of Eq. (1) to the data in Fig. 5 (shown in the plot) yields $n=2.89\pm0.20$, consistent with three-photon absorption. Using the parameter A to convert the transmission signal to percent of transmission yielded physically plausible values of 35%–92% over the range of pulse energies probed.

The data at 800 nm are consistent with a third-order absorption process. In view of the higher photon energies at 400 and 267 nm, it is reasonable to expect second-order absorption at 400 nm and first-order absorption at 267 nm. A progression from third-order absorption at 800 nm processes to first order absorption at 267 is consistent with the dramatic drop in pulse energy required for darkening as the wavelength is decreased.

E. Other alkali silicate glasses

Experiments with pure alkali silicate glasses, including $LiO_2\cdot 3SiO_2$, $NaO_2\cdot 3SiO_2$, and $KO_2\cdot 3SiO_2$ show similar darkening behavior. A comparison of the resulting absorption spectra for these glasses and soda-lime glass is shown in Fig. 6. Significantly, the optical density due to coloration increases dramatically as the diameter of the alkali increases from Li to Na to K. Although the nonalkali components in commercial glass slides may play a role in darkening soda-lime glass, alkali alone is sufficient. Again, all of these alkali glasses are darkened at pulse energies well below those required for supercontinuum emission, suggesting that supercontinuum emission is not involved in the darkening process.

F. Onset of transmission drop

The initial drop in the transmission signal of Fig. 3 is rate limited by the response time of the detection electronics. With a significant loss in sensitivity, nanosecond transmission measurements can be made. Adequate signals were obtained by probing the transmission at 473 nm using light from a cw laser diode while exposing the glass to 200 μJ pulses of 400-nm femtosecond laser light. The resulting transmission signal, averaged over several laser pulses, appears in Fig. 7(a). The initial transmission drop in Fig. 7(a) is still rate limited by the response time of the electronics, about 10 ns. The positive going transient at time $t=0$ also appears in signals detected in the absence of a sample [inset in Fig. 7(a)], and is attributed to scattered 400-nm light from the femtosecond pulse.

In the microsecond time-scale measurements of Fig. 7(b), the transmission signal drops immediately and begins to recover no later than 1 μs after the femtosecond pulse. The white line through the data shows a least squares fit of the form $I=I_o+\alpha t^{0.5}$ to the data. This function is the small

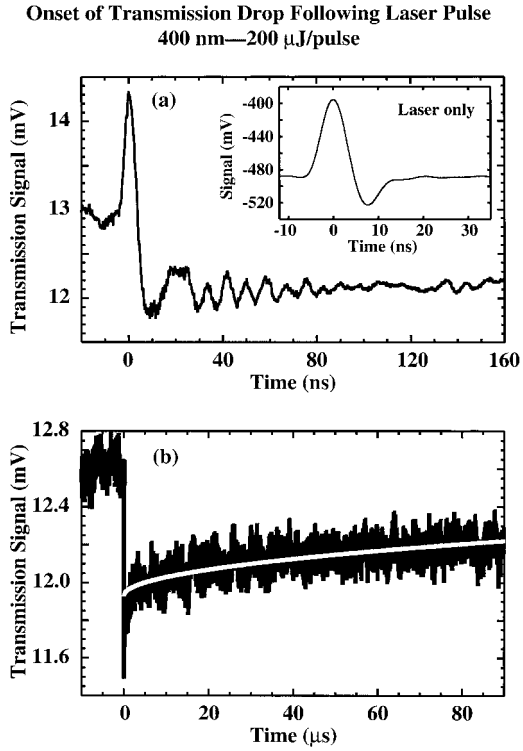

FIG. 7. Averaged photodiode signals due to the transmission of CW 473-nm photodiode laser beam on nanosecond and microsecond time scales following several 400-nm femtosecond laser pulses. (a) Nanosecond time-scale measurement and (b) microsecond time-scale measurements. The ns time-scale measurements of (a) are rate limited by the 10-ns time response of the electronics. The inset of (a) shows the photodiode signal recorded in the absence of a sample, suggesting that the positive going transient in (a) is due to scattered light from the femtosecond pulse.

time limit of the stretched exponential function used to describe the recovery of transmission signals on millisecond time scales (described below).

Although these transmission measurements involve different probe and pump wavelengths, they suggest that the initial drop in transmission represented in Fig. 3(b) takes place on time scales of less than 10 ns. The subsequent recovery of the transmission signal, when observed, begins within 1 μs of the femtosecond laser pulse. Measurements with higher time resolution using pump-probe techniques are in progress.

IV. DISCUSSION

A third-order absorption process at 800 nm (4.6 eV) is well into the strong UV absorption in soda-lime glass; sufficiently intense ultrafast laser pulses would then produce high densities of electron hole pairs. We argue that the trapping, detrapping, and recombination of these excitations account for the time behavior of the observed darkening and partial recovery, both on slow time scales (seconds, multipulse exposure) and on fast time scales (microseconds, single-pulse exposure).

A. Role of hole traps

As shown in Fig. 2, the absorption spectrum of soda-lime glass darkened with femtosecond laser radiation is very

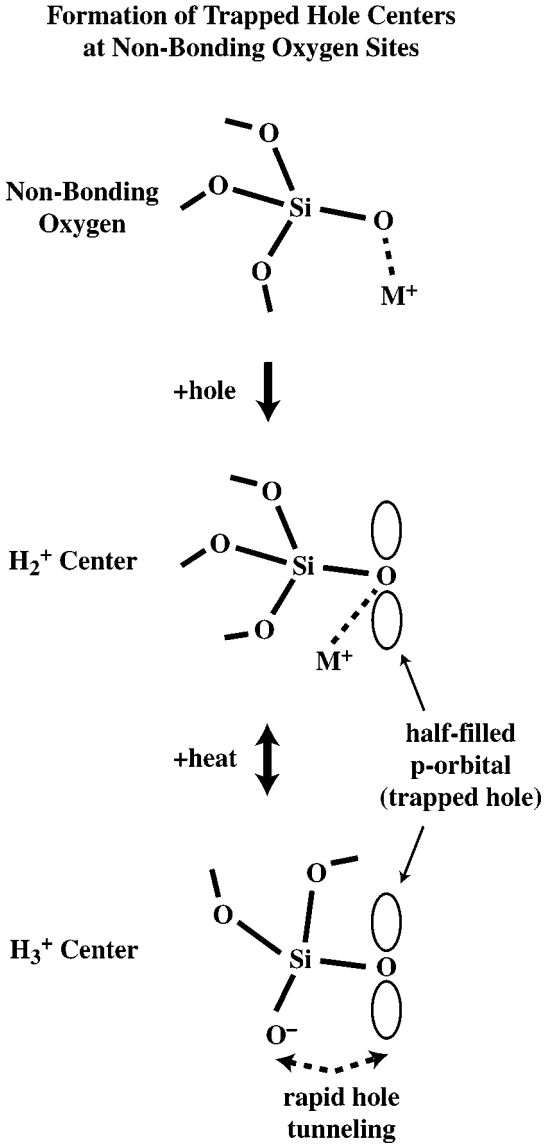

FIG. 8. Schematic of proposed mechanism for the production of H_3^+ centers at nonbonding oxygen sites in soda-lime glass. The H_2^+ center is a NBO with one trapped hole and an alkali nearby; a possible structure for the H_3^+ center is two NBOs on the same Si with one trapped hole and the alkali removed.

similar to the absorption of glass darkened with x rays (and γ rays). Both darkened samples show broad absorption peaks centered at about 460 and 620 nm. Spin resonance measurements of pure sodium silicate glasses exposed to x and γ radiation have associated these peaks with trapped hole centers. The absorption centered near 460 nm is due to H_2^+ centers (or OHC_1 centers); the absorption centered near 620 nm is due to H_3^+ centers (or OHC_2 centers).[7–10] Similar absorption peaks are observed in alkali aluminosilicate glasses, suggesting that the basic defect geometries are the same, with aluminum substituting for some of the silicon.[9] Recent studies show that significant nonbonding oxygen (NBO) densities can be present in aluminosilicate glasses, contrary to previous predictions.[11]

On the basis of previous work on alkali silicate glasses exposed to x and γ radiation, we suggest that the defects

responsible for persistent absorption at 633 nm are primarily H_3^+ centers with absorption centered near 620 nm. Some contribution is expected from H_2^+ centers, which exhibit broad absorption centered near 460 nm.[7,8,10] A diagram illustrating the expected structure of these two defects appears in Fig. 8. The H_2^+ center forms when a hole is trapped at a NBO.[10,12] Electron spin resonance (ESR) measurements in conjunction with molecular dynamics simulations suggest that most NBOs are charge compensated by a nearby alkali ion.[10] The alkali relaxes significantly away from the NBO when the hole is trapped.

Although the structure of the H_3^+ center has not been determined with certainty, the principal candidate structures involve a silicate tetrahedron with two NBOs.[10] The coupling between the H_3^+ center and surrounding alkali is weaker than in the H_2^+ center. ESR data require that the two NBOs of the H_3^+ center be magnetically equivalent on time scales greater than milliseconds. The data are consistent with rapid tunneling of the hole from one equivalent NBO to the other on time scales of 1–50 ps. (The magnetic equivalence in an analogous trapped hole center in fused silica also involves rapid tunneling of an electron between two NBOs.[13]) Alkali migration toward one of these NBOs would break the symmetry and converts a H_3^+ center back to a H_2^+-like center.

Bleaching studies indicate that the H_2^+ and H_3^+ centers are reversibly converted from one into the other at room temperature; thus the two centers densities are normally in thermal equilibrium.[7] H_3^+ centers are much more vulnerable than H_2^+ centers to destruction by electron recombination and bleaching effects.[7] At liquid nitrogen temperature, illumination into the 620 nm band bleaches the H_3^+ centers (as well as the E_3^- band at 310 nm due to an electron trap). In contrast, visible radiation has little effect on the H_2^+ centers at liquid nitrogen temperature. When samples depleted in H_3^+ centers at liquid nitrogen temperature are subsequently heated to room temperature, the H_3^+ absorption is partially restored by the conversion of H_2^+ centers to H_3^+ centers.[7] In summary, H_3^+ center production requires (1) nonbonding oxygen sites, (2) holes for trapping at NBOs, and possibly (3) H_2^+ centers for subsequent conversion to H_3^+ centers.

While it is possible that some H_3^+ centers form directly by hole trapping at suitable precursor sites (silicate tetrahedra with two NBOs and no nearby alkali), we expect that most of the H_3^+ centers form by thermal conversion of H_2^+ centers. The formation of H_2^+ centers requires little structural modification, and the potential H_2^+ center precursors (simple NBOs) far outnumber the potential H_3^+ precursors (double NBOs).

B. Role of electron traps

The hole centers responsible for absorption at 633 nm would not be stable against electron-hole recombination in the absence of stable electron traps. In soda silicate glasses exposed to ionizing radiation at room temperature, electron traps (denoted E_3^- and E_4^- centers) are responsible for the enhanced absorption in the near UV.[7,8] We observe similar absorption in both the femtosecond and x-ray irradiated glasses, shown in Fig. 2. The E_3^- center in particular is associated with an absorption peak centered at about 310 nm.[7,8] Optical absorption measurements on x-irradiated glass show a close correlation between the density of E_3^- centers, on the one hand, and the density of H_2^+ and H_3^+ centers, on the other. Cohen and Janezic concluded that the these three centers were produced by the same absorption event (e.g., by the creation of electron-hole pairs).[8] The electrons corresponding to the holes trapped at H_2^+ and H_3^+ centers are primarily trapped at E_3^- centers. Maintaining this separation of charge is necessary for long term coloration of the glass.

At liquid nitrogen temperature, composite absorption bands centered near 680 and 600 nm are attributed mainly to electron traps denoted E_1^- and E_2^- centers respectively.[7] Although these centers do not appear in our absorption spectra acquired at room temperature, they could constitute short-lived absorption centers at room temperature. Since the coloration produced in the initial stages of femtosecond irradiation is stable on millisecond time scales, transient electron traps are not responsible for this coloration.

C. Role of recombination

If the observed darkening is due to excitations created by third-order photon absorption events, the 15th order dependence of the transmission drop on the pulse energy indicates that about five excitations are required to generate a single, stable H_3^+ center. This high number would seem to rule out interactions between simple, mobile excitations. However, the inhomogeneous structure of sodium silicate glasses and the high excitation densities produced by femtosecond lasers can allow decay schemes that produce stable, occupied electron and hole traps. Although the proposed scheme is somewhat conjectural, it indicates how the glass structure, in conjunction with high excitation densities, can yield extremely nonlinear darkening behavior.

Molecular dynamics simulations indicate that the alkali and NBOs are not distributed randomly throughout the glass, but instead cluster.[14–18] This result is supported by studies of magnetic resonance,[19] extended x-ray fine structure,[20] and neutron diffraction. Even at alkali concentrations as low as 10%, each NBO is associated with at least two alkali ions,[14] and often with three or four alkali.[15] Localized electron states in the NBOs constitute the upper edge of the valence band of sodium silicate glasses.[16] Similarly, unoccupied (nonlocalized) electron states on the alkali ions constitute the bottom of the conduction band.[16] The creation of exciton-like excitations would most likely be confined to these alkali-NBO channels. Mobile excitations created elsewhere would soon be localized along these channels.

It is likely that the excitations created initially by the femtosecond laser would be similar to Frenkel excitons, localized electron-hole pairs where the hole would quickly localize on a NBO and the electron on a nearby alkali ion. In the normal course of events, these excitations would recombine with high efficiency via tunneling interactions. At high excitation densities, however, there may be a significant probability that an electron associated with one excitation will recombine with a hole on a nearby excitation. This situation is illustrated schematically in Fig. 9.

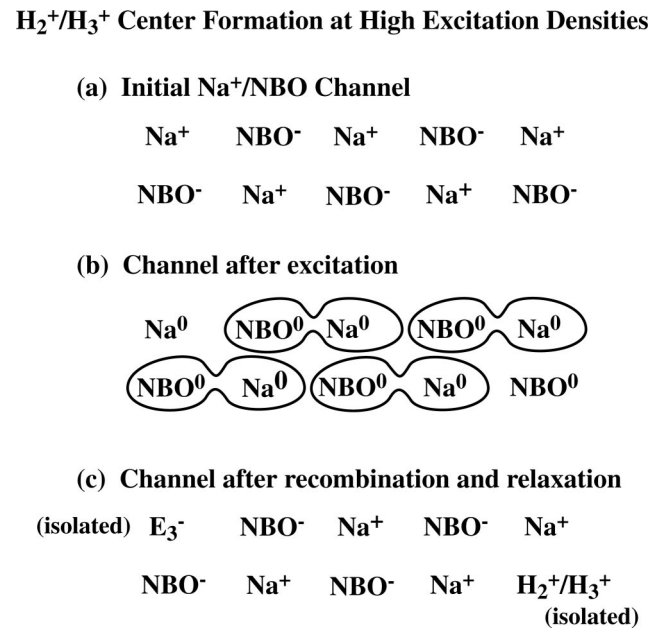

FIG. 9. Schematic illustration of the decay of excitations along a Na^+/NBO channel in soda-lime glass to form stable, isolated, and occupied electron and hole traps. (a) Na^+/NBO channel prior to the first laser pulse; Na^+/NBO clusters are favored sites for excitation. (b) The femtosecond laser pulse produces high densities of Frenkel exciton-like excitations. When electrons produced in one excitation event recombine with holes produced in another, a few defects become isolated from defects of opposite sign and therefore fail to recombine. (c) The pairwise recombination indicated in (b) produces isolated electron and hole defects at the edges of the cluster. Subsequent lattice relaxation traps the electron and hole to form the observed absorption centers.

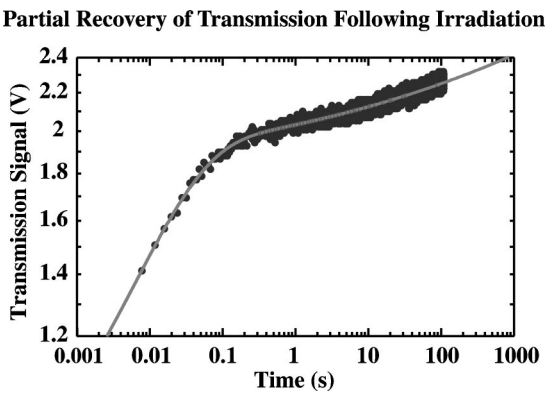

FIG. 10. Partial recovery of the transmission signal after a darkening experiment plotted on a log–log scale. Darkening was achieved by exposure to 800 nm femtosecond laser radiation for 80 s with 1000 pulses per second at 930 μJ per pulse. The femtosecond laser beam was blocked at $t=0$ and remained blocked for the remainder of data collection. The broad gray line shows the best fit of the data to Eq. (2), which represents the sum of stretched exponential and power-law behavior.

A schematic illustration of a Na^+/NBO channel appears in Fig. 9(a). For simplicity, we present the simple case where each Na^+ has two NBO nearest neighbors, and vice versa. Given sufficient excitation densities, clusters of exciton-like defects would form, in which an electron from each NBO is transferred to a nearby NBO. This situation is presented in Fig. 9(b). Electron-hole recombination will most often return the channel to its original state; in Fig. 9(b), this would involve pairwise recombination vertically. However, if recombination occurs by pairs horizontally, nominally isolated charge carriers are produced at each end of the channel. Given the channel structure, horizontal and vertical recombination would occur with similar probabily. Lattice relaxation around the isolated charges would then produce E_3^- and H_2^+/H_3^+ center pairs, as indicated in Fig. 9(c). The hole center is the designated H_2^+/H_3^+ center to reflect the thermal activated conversion of one center into the other. Given the relatively low density of symmetric, double NBO configurations in soda-lime glass (required for H_3^+ centers), we expect that H_2^+ centers are produced initially.

The stability of the resulting defect configuration depends strongly on the distance between nearby E_3^- and H_2^+/H_3^+ center pairs. Closely spaced pairs are vulnerable to decay by tunneling processes. A minimum of three adjacent (where the word adjacent is used loosely) excitations is necessary to allow a final defect configuration that is more stable than a single, isolated excitation. The high order fluence dependence of the darkening process suggests that about five adjacent excitations are required to produce stable defect configurations. The necessity for high excitation densities accounts for the difficulty of darkening soda-lime glass with excimer lasers at much higher pulse energies. Assuming that the excitation lifetime is significantly less than the 10–30 ns pulse widths of excimer lasers, the requisite excitation densities are seldom achieved.

Subsequent femtosecond laser pulses will produce excitations along Na^+/NBO channels populated with E_3^- and H_2^+/H_3^+ center. As long as the density of H_2^+/H_3^+ centers is low, the main effect of subsequent irradiation will be to produce additional centers. In the above work, this corresponds to the low dose region where transmission changes from pulse to pulse were cumulative and persistent. Assuming that excitations are not produced at the E_3^- and H_2^+/H_3^+ center sites themselves, the decay of these excitations will usually leave behind an equal or greater number of E_3^- and H_2^+/H_3^+ centers, often at different positions. Eventually, the average distance between H_2^+/H_3^+ and E_3^- centers will drop to the point where tunneling recombination between these centers becomes significant on millisecond time scales. The high cross section of H_3^+ centers for electron interactions will render them more vulnerable to tunneling events than the H_2^+ centers. These tunneling events would account for the rise in transmission (partial bleaching) following the laser pulse, e.g., as seen in Fig. 3(b).

The importance of recombination is supported by transmission measurements on second time scales after femtosecond laser radiation is terminated. Figure 10 shows a log–log plot of the transmission signal versus the time after exposure to 800 nm femtosecond laser radiation is terminated. These measurements span four orders of magnitude in time. At somewhat longer times, the transmission stabilizes. (The absorption spectra in Fig. 2 were taken several minutes after exposure and did not change over time.) The partial bleaching or recovery is continuation of the electron-hole recombination that occurs between laser pulses. The recovery shows a marked transition to slower kinetics about 100 ms after illumination stops. The form of this transition suggests a

stretched exponential function, which is often associated with transport in random networks.[21] The very slow recovery at long times (more than 1 s after illumination stops) suggests a power law in time.

The data in Fig. 10 are well described by a function of the form

$$T(t)=A+B\left\{1-\exp\left[-\left(\frac{t}{\tau}\right)^{\beta}\right]\right\}+Ct^{\beta/4}, \tag{2}$$

with $\beta=0.5$ and $\tau=13$ ms.

The constant A represents the initial value of the transmission signal (at time $t=0$). The second term represents the increase in transmission at short times ($t<$a few seconds) due to the destruction of absorption centers by electron-hole recombination in the form of a stretched exponential. Stretched exponential kinetics in amorphous materials often reflect slow defect transport due to retrapping or limited dimensionality.[21] An exponential tail of states extending into the band gap from the conduction band can provide a wide range of trap depths for mobile charge in amorphous solids. Charge trapped in the low-lying states is not readily freed. This charge has a disproportionate effect on charge transport, and leads to stretched exponential kinetics.[21] Charge transport is also slowed when transport is confined to low-dimension structures.[22–24] The sodium-rich channels in alkali glasses would provide such low-dimension structures. The value of β in Eq. (2) is constrained by details of charge transport. β reflects the trap depth distribution in retrapping limited recombination, and the dimensionality of the transport channels in dimension limited recombination. If the recombination mechanism is understood, the decay kinetics can provide important information on the electronic and chemical structure of amorphous solids.

In the short time limit, the stretched exponential term in Eq. (2) increases as $t^{0.5}$. The transmission data of Fig. 7(b), acquired on microsecond time scales, also increases with the square root of time. This suggests that the recombination processes responsible for rise in transmission after irradiation follows stretched exponential kinetics for up to six orders of magnitude in time (1 μs to 1s).

The third term in Eq. (2) represents power law kinetics at long times ($t>$a few seconds in Fig. 10). We attribute the transition to slow, power-law kinetics to inhomogeneities in the defect distribution that develop as recombination proceeds. As nanometer-scale volumes of glass become depleted in recombination centers, mobile charge in these regions experiences longer survival times.[22–24] The recombination kinetics in this long-time limit are often simply related to the kinetics at shorter times. This is reflected in Eq. (2) by fixing the exponent in the power-law term to a fixed multiple of β. Despite the gradual increase in transmission shown in Fig. 10, significant absorption remains for very long times (at least months). In many other systems that show similar recovery kinetics, the average defect lifetime is in fact infinite.[21]

The release and transport of the charge carriers is most likely thermally driven. Heating darkened glass to ~200 °C quickly bleaches the visible darkening. Similar thermal bleaching of colored sodium silicate glass was mentioned by Efimov *et al.*[6] We plan to perform a study of the darkening and bleaching kinetics versus the temperature in the near future.

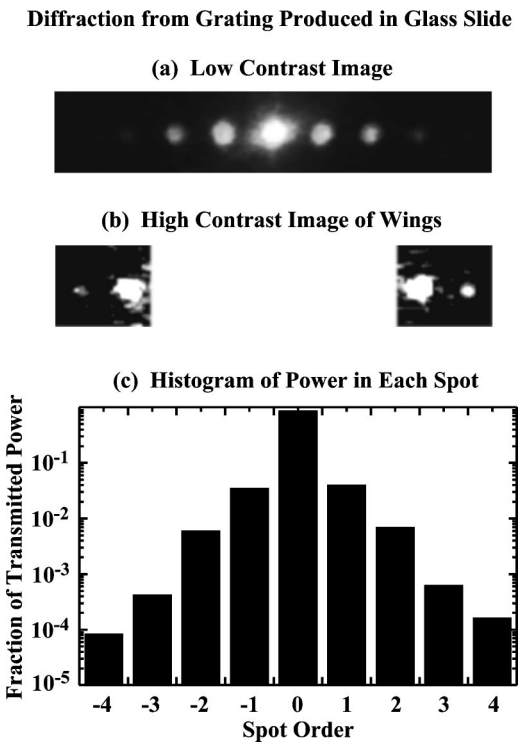

FIG. 11. (a) Low contrast image of a diffraction pattern produced by the diffraction of a cw He:Ne beam from a grating produced in a soda-lime glass slide by femtosecond pulses of 800 nm radiation. (b) High contrast image showing higher order spots. (c) Histogram of the fraction of the total transmitted power found in each spot of the diffraction pattern.

D. Grating formation

Highly nonlinear effects similar to the darkening in soda-lime glass are often useful for patterning transparent materials. Nonlinear material responses allow the production of well-defined features with sharp edges, sometimes with feature sizes smaller than the nominal diffraction limit.[25,26] We can pattern a grating using this darkening mechanism with femtosecond, 800 nm laser pulses by splitting the beam into two equal intensity beams that are allowed to interfere at an angle θ. Figure 11 shows the center and higher order spots out to fourth order produced when the 633 nm beam from a He:Ne laser is diffracted by a grating produced by the interference of two femtosecond, 800 nm laser beams converging at an angle $\theta=1.3°$. This geometry is expected to produce dark strips with spacing $\Lambda=\lambda_0/2\sin\theta$, where λ_0 is the wavelength used to write the pattern. The predicted grating spacing is therefore $\Lambda=35$ μm. The diffraction pattern displayed in Fig. 11 is consistent with $\Lambda-36$ μm, in agreement with the predicted value. The radiant intensity in the diffracted beams makes up 10.5% of the total intensity transmitted. The formation of other robust, long-lived patterns by exposure to spatially modulated laser radiation is being pursued and may suggest additional applications.

V. CONCLUSION

Femtosecond laser pulses generated high excitation densities in soda-lime glass at all three laser wavelengths employed in this work. The extremely strong dependence of darkening on the pulse energy was only partly due to nonlinear absorption effects. In soda-lime glass at 800 nm, we observed three-photon absorption, whereas the dependence of coloration on pulse energy is extreme ($\sim$15th order). This is explained by the strong dependence of defect production on the density of excitations (electron-hole pairs). Thus strong (fourth to fifth order) nonlinear effects are observed even at 267 nm, where single photon absorption dominates. A model was presented in which clusters of excitations decay in such a way as to produce separated E_3^- and H_2^+ pairs. Thermally activated conversion of H_2^+ to H_3^+ centers generates most of the absorption at 633 nm. On longer time scales we observe slow partial bleaching with stretched exponential kinetics due to charge transport and recombination among these electron and hole centers. Analysis of the kinetics of darkening and bleaching can provide a useful probe of electronic and chemical structure of this amorphous material. Finally, we show that pattern formation (i.e., to produce a grating) in soda-lime glass can be readily achieved. In progress are experiments on a series of alkali silicates, including Rb and Cs, experiments on the effect of adding aluminum to soda glass, pump-probe experiments to monitor the kinetics of defect production and annhilation on subpicosecond time scales, and experiments to explore in detail the effect of temperature on the kinetics of both darkening and bleaching.

ACKNOWLEDGMENTS

This work was supported by the Department of Energy under Contract No. DE-FG03-98ER14864 and by a Major Research Instrumentation grant from the National Science Foundation under Contract No. DMR 00-79774.

[1] R. L. Webb, L. C. Jensen, S. C. Langford, and J. T. Dickinson, J. Appl. Phys. **74**, 2323 (1993).
[2] J. T. Dickinson, L. C. Jensen, R. L. Webb, M. L. Dawes, and S. C. Langford, J. Appl. Phys. **74**, 3758 (1993).
[3] J. J. Shin, M.-W. Kim, and J. T. Dickinson, J. Appl. Phys. **80**, 7065 (1996).
[4] J. T. Dickinson, S. C. Langford, L. C. Jensen, P. A. Eschbach, L. R. Pederson, and D. R. Baer, J. Appl. Phys. **68**, 1831 (1990).
[5] M. L. Dawes, W. Hess, Y. Kawaguchi, S. C. Langford, and J. T. Dickinson, Appl. Phys. A: Mater. Sci. Process. **69**, S547 (1999).
[6] O. M. Efimov, L. B. Glebov, S. Grantham, and M. Richardson, J. Non-Cryst. Solids **253**, 58 (1999).
[7] J. H. Mackey, H. L. Smith, and A. Halperin, J. Phys. Chem. Solids **27**, 1759 (1966).
[8] A. J. Cohen and G. G. Janezic, Phys. Status Solidi A **77**, 619 (1983).
[9] G. H. Sigel, Jr., J. Non-Cryst. Solids **13**, 372 (1973/74).
[10] I. A. Shkrob, B. M. Tadjikov, and A. D. Trifunac, J. Non-Cryst. Solids **262**, 35 (2000).
[11] J. F. Stebbins and X. Zhi, Nature (London) **390**, 60 (1997).
[12] D. L. Griscom, J. Non-Cryst. Solids **40**, 211 (1980).
[13] K. S. Song and R. T. Williams, *Self-Trapped Excitons* (Springer, Berlin, 1993).
[14] T. F. Soules, J. Chem. Phys. **71**, 4570 (1979).
[15] S. K. Mitra and R. W. Hockney, Philos. Mag. B **48**, 151 (1983).
[16] R. A. Murray and W. Y. Ching, J. Non-Cryst. Solids **94**, 144 (1987).
[17] R. G. Newell, B. P. Feuston, and S. H. Garofalini, J. Mater. Res. **4**, 434 (1989).
[18] C. Huang and A. N. Cormack, J. Chem. Phys. **93**, 8180 (1990).
[19] R. Dupree, D. Holland, and D. S. Williams, J. Non-Cryst. Solids **81**, 185 (1986).
[20] G. N. Greaves, A. Fontaine, P. Lagarde, D. Raoux, and S. J. Gurman, Nature (London) **293**, 611 (1981).
[21] H. Scher, M. F. Shlesinger, and J. T. Bendler, Phys. Today **44**, 26 (1991).
[22] G. Zumofen, A. Blumen, and J. Klafter, J. Chem. Phys. **82**, 3198 (1985).
[23] H. Schnörer, V. Kuzovkov, and A. Blumen, J. Chem. Phys. **92**, 2310 (1990).
[24] H. Schnörer, V. Kuzovkov, and A. Blumen, J. Chem. Phys. **93**, 7148 (1990).
[25] H. Jiang, Z. Wu, Z. Zhang, Q. Sun, H. Yang, and Q. Gong, Opt. Express **10**, 1244 (2002).
[26] J. Krüger and W. Kautek, Laser Phys. **9**, 30 (1999).